Published in final edited form as:
Clin Cancer Res. 2008 December 15; 14(24): 8094–8101. doi:10.1158/1078-0432.CCR-08-0703.

Inhibition of mTOR by Rapamycin Causes the Regression of Carcinogen-Induced Skin Tumor Lesions

Panomwat Amornphimoltham, **Kantima Leelahavanichkul**, **Alfredo Molinolo**, **Vyomesh Patel**, and **J. Silvio Gutkind***
Oral & Pharyngeal Cancer Branch, National Institute of Craniofacial and Dental Research, National Institutes of Health, Bethesda, MD 20892

Abstract

Purpose—The activation of Akt/mammalian target of rapamycin (mTOR) pathway represents a frequent event in squamous cell carcinoma (SCC) progression, thus raising the possibility of using specific mTOR inhibitors for the treatment of SCC patients. In this regard, blockade of mTOR with rapamycin prevents the growth of human head and neck SCC cells when xenotransplanted into immunodeficient mice. However, therapeutic responses in xenograft tumors are not always predictive of clinical anti-cancer activity.

Experimental Design—As genetically defined and chemically-induced animal cancer models often reflect better the complexity of the clinical setting, we used here a two-step chemical carcinogenesis model to explore the effectiveness of rapamycin for the treatment of skin SCC.

Results—Rapamycin exerted a remarkable anti-cancer activity in this chemically-induced cancer model, decreasing the tumor burden of mice harboring early and advanced tumor lesions, and even recurrent skin SCCs. Immunohistochemical studies on tumor biopsies and clustering analysis revealed that rapamycin causes the rapid decrease in the phosphorylation status of mTOR targets, followed by the apoptotic death of cancer cells and the reduction in the growth and metabolic activity of the surviving ones, concomitant with a decrease in the population of cancer cells expressing mutant p53. This approach enabled investigating the relationship among molecular changes caused by mTOR inhibition, thus helping identify relevant biomarkers for monitoring the effectiveness of mTOR inhibition in the clinical setting.

Conclusions—Together, these findings provide a strong rationale for the early evaluation of mTOR inhibitors as a molecular targeted approach to treat SCC.

Keywords

rapamycin; carcinogenesis; squamous cell carcinoma; mTOR; molecular targets

Introduction

Cancer arises in multistep process resulting from the sequential accumulation of genetic defects and the clonal expansion of selective cell populations (1)(1). For example, in the case of human head and neck squamous carcinomas (HNSCC), tumor progression often involves the sequential genetic or epigenetic inactivation of multiple tumor suppressor genes, such as *p16* (9p21), *APC* (5q21-22) and *p53* (17p13) (2), concomitant with changes

*To whom requests for reprints should be addressed, Oral and Pharyngeal Cancer Branch, National Institute of Dental and Craniofacial Research, National Institutes of Health, 30 Convent Drive, Building 30, Room 212, Bethesda, Maryland 20892-4330. Phone: (301) 496-6259; Fax: (301) 402-0823; sg39v@nih.gov.

in the activation state of signaling pathways that promote the aberrant growth of the cancerous cells. The later frequently result from the over-expression and/or activity of cell surface receptors, including epidermal growth factor receptors (EGFR), hepatocyte growth factor receptors (c-Met), and receptors for numerous cytokines, chemokines, and inflammatory mediators (3-5). These receptors share the ability to promote the activation of a number of intracellular signaling pathways, including the Ras-mitogen-activated protein kinase kinase (MEK)-extracellular signal-regulated kinase (ERK) biochemical route, and the phosphatidylinositol (PI)-3-kinase (PI3K)-Akt-mammalian target of rapamycin (mTOR) pathway, which in turn promote cell proliferation and survival (6). This emerging knowledge on the nature of the signaling networks driving the unrestricted growth of cancerous cells has now enabled the development of novel therapies targeting key signaling molecules whose dysregulation contribute to tumor progression in each cancer type.

In particular, the widespread activation of the PI3K/AKT/mTOR pathway in HNSCC progression has raised the possibility of using specific mTOR inhibitors and their derivatives for the treatment of HNSCC patients (7, 8). In this regard, blockade of mTOR with rapamycin exerts a potent anti-tumoral effect and even prevents minimal residual disease in a number of human HNSCC xenograft models (9-11).

However, effectiveness in human xenograft tumors is not always predictive of a clinical anti-cancer activity (12, 13). Genetically defined and chemically induced animal cancer models are often more difficult to treat than xenotransplanted human tumors in immunocompromised mice, but reflect better the more complex and challenging situation of the clinical setting (12-14). Thus, in this study, we took advantage of the well-established two-step chemical carcinogenesis model, in which squamous carcinogenesis (SCC) is initiated by the topical application of a tobacco-related chemical carcinogen (DMBA) to the skin followed by the prolonged treatment with phorbol esters (TPA) (15), to explore the effectiveness of rapamycin for the treatment of skin SCC lesions. We show here that rapamycin exerts a potent anti-cancer activity in this chemically induced cancer model, as chronic administration of rapamycin decreases the tumor burden of mice harboring early and advanced primary tumor lesions and even recurrent SCC. Indeed, the inhibition of mTOR with rapamycin results in the regression of carcinogen-induced skin SCC, thus providing a strong rationale for the early clinical evaluation of rapamycin and its derivatives in SCC patients.

Materials and Methods

Reagents

7,12-dimethyl-benz[*a*]anthracene (DMBA) was purchased from Sigma (St. Louis, MO); phorbol ester 12-*O*-tetradecanoylphorbol-13-acetate (TPA) from Alexis Biochemicals (San Diego, CA). Rapamycin was provided by the Developmental Therapeutics Program (NCI).

Antibodies

Polyclonal rabbit antibodies against phospho-Akt (S473), phospho-S6, eIF4E, and Cyclin D1 were purchased from Cell Signaling (Danvers, MA). Rat monoclonal anti-mouse CD31 (BD Pharmingen; San Diego, CA), polyclonal rabbit anti mouse CD3 (Dako; Carpinteria, CA), rat monoclonal anti F4/80 (Serotec; Raleigh, NC), rabbit polyclonal anti p53 (Novocastra; Norwell MA), rabbit polyclonal anti Glut1, (Chemicon; Temecula, CA), polyclonal rabbit anti VEGF (Santa Cruz; Santa Cruz, CA), and mouse monoclonal anti PCNA (Zymed; Carlsbad, CA), were used when indicated.

Animals

All animal studies were carried out according to NIH approved protocols, in compliance with the Guide for the Care and Use of Laboratory Animals. Six-week-old female FVB/N mice were obtained from the Taconic Farm, Inc. (Hudson, NY), housed in appropriate sterile filter-capped cages and fed and watered *ad libitum*. All handling, tumor induction and treatment procedures were conducted in a laminar-flow biosafety hood.

Tumor induction and rapamycin treatment

Mice were shaved in the back and tumors initiated by the topical treatment with a single dose of DMBA (100 μg/200 μl in acetone), followed by the tumor promotion phase in which mice were treated twice weekly with TPA (12.5 μg/200 μl in acetone) for 24 weeks. The number and diameter of each tumor was measured weekly. Rapamycin treatment was started when papillomas were first observed for the study of early lesion, approximately 9-10 weeks after the initiation, or once the tumors achieved the indicated tumor burden for advanced lesions (16-18 weeks). Drug administration of tumor-bearing animals was essentially performed as previously described (7). Briefly, tumor bearing animals were randomly divided into two groups and treated with rapamycin (10 mg/kg/day) or an equal volume of diluent (an aqueous solution of 5.2% Tween-80 and 5.2% PEG). For early lesions, treatment schedule was a single injection per animal, per day, given intraperitoneal, for 5 consecutive days. For advanced and recurrent lesions, rapamycin was administered daily until the end of the study. Animals from each group were euthanized for tissue retrieval at the indicated time points. Tumor tissues were immediately collected after sacrificed and fixed in buffered zinc-formalin (Z-fix, Anatech, MI) at room temperature for 12 hours. The tissues were then transferred to alcohol 70% and processed for paraffin embedding for histopathological and immunohistochemical analysis.

Immunohistochemistry (IHC)

The tissues slides were deparaffinized in xylene, hydrated through graded alcohols and distilled water, and rinsed with PBS. Antigen retrieval was performed using a citrate buffer (pH 6) in a microwave for 20 minutes (2 minutes at 100% power and 18 minutes at 10% power). Slides were allowed to cool down for 30 minutes, rinsed twice with PBS, and incubated in 3% hydrogen peroxide in PBS for 10 minutes to quench the endogenous peroxidase. The sections were then washed in distilled water and PBS and incubated in blocking solution (2% BSA in PBS-1% Tween20) for 1 hour at room temperature. Excess solution was discarded and the sections were incubated with the primary antibody diluted in blocking solution at 4°C, overnight. After washing with PBS, the slides were sequentially incubated with the biotinylated secondary antibody (Vector Laboratories, 1:400) for 30 min, followed by the ABC complex (Vector Stain Elite, ABC kit, Vector Laboratories) for 30 min at room temperature. The slides were washed and developed in 3,3-diaminobenzidine (Sigma FASTDAB tablet, Sigma Chemical, St. Louis, MO) under microscopic observation. The reaction was stopped in tap water and the tissues counterstained with Mayer's hematoxylin, dehydrated and mounted. The images were taken using a Carl Zeiss Axioplan 2 microscope (Carl Zeiss Inc. North America). The evaluation of the IHC was conducted blindly, without knowledge of the origin and status of the treatment. The whole tissues were examined and classified based on the staining intensity (1, weak staining; 2, moderate staining; and 3, strong staining), and the percentage of positive cells (0, less than 10% of stained cells; 1, between 10 and 25%; 2, between 25 and 50%; 3, 50 to 75%; and 4, 75% to 100% of cells stained). Results were scored by multiplying the percentage of positive cells by the intensity (7, 16).

Immunofluorescence (IF) double staining

The OCT embedded tissues were cut onto the silanated glass slides at 15 μm thickness with cryostat, air-dried and stored at −80 °C. To process for IF staining, the cryosections were thawed at room temperature, hydrated in distilled water, and washed thoroughly with PBS. The sections were then incubated in the blocking solution (5% heated-inactivated goat serum in 0.1% triton X-100 PBS) for 1 h at room temperature. Excess solution was discarded and the sections incubated with the first primary antibody diluted 1:100 in blocking solutions at 4°C, overnight. After washing with PBS the slides were sequentially incubated with the biotinylated secondary antibody (Vector Laboratories, 1:300) for 1 h, followed by the Texas-red avidin antibody (Vector Stain Elite, ABC kit, Vector Laboratories) for 30 min at room temperature. The slides were washed and incubated in avidin/biotin blocking kit (Vector Laboratories) for 15 min each, followed by incubation in the blocking solution before repeated the staining process with the second primary antibody as described above. The fluorescein-labeled antibody against species of primary antibody was used as secondary antibody. The tissues were then mounted in Vectashield mounting medium with DAPI (Vector Laboratories).

p53 mutation analysis

Tumors from vehicle and rapamycin-treated mice (1-7 days treatment) were subjected to mutation analysis of *p53*. Exons 4-9 of *p53* were amplified by polymerase chain reaction from genomic DNA (10-50 ng per reaction) with specific oligonucleotide primers. The primers used for PCR are as follows: exon 4 sense 5′TAGGCTGAGAACACAGTCCTGAGG3′ and anti-sense 5′GCATTGAAAGGTCACACGAAAGAC3; exon 5 sense 5′CCTGATCGTTACTCGGCTTGTC3′ and anti-sense 5′CAACTGTCTCTAAGACGCACAAACC3′; exon 7 sense 5′TGTAGTGAGGTAGGGAGCGACTTC 3′ and anti-sense 5′GGGTAGGAACCAAAGAGCGTT3′; exon 8+9 sense 5′GCAGATATGACAAGAGGGGTTG 3′ and anti-sense 5′GCGAGAGACAGAGGCAATAAGG 3′. PCR products were sequenced directly in both directions with a 3730 DNA Analyzer (Applied Biosystems, Foster City, CA). Sequence traces were assembled and analyzed to identify potential genomic alterations using the Mutation Explorer software package (SoftGenetics, State College, PA) when compared with the sequence for all annotated exons and adjacent intronic sequences extracted from Reference assembly NCBI database (NT_096135.5; http://www.ncbi.nlm.nih.gov/).

Terminal nucleotidyl transferase-mediated nick end labeling (TUNEL) assay

The tissue sections were dewaxed in xylene and rehydrated in graded ethanol and distilled water. After washing thrice with PBS, the slides were incubated with proteinase K (Qiagen, Valencia, CA; 20 μg/mL in PBS) for 20 min at room temperature, and the TUNEL staining was carried out using the *In situ* Cell Death Detection; Texas red Kit (Boehringer Mannheim Biochemicals, Indianapolis, IN) according to the manufacturer's instructions. The tissues were then mounted in Vectashield mounting medium with DAPI (Vector Laboratories).

Retro-orbital blood collection

The retro-orbital blood collection from medial canthus was performed as described in NIH animal protocol and guideline. Briefly, a microhematocrit tube was inserted through the conjunctiva and into the orbital sinus by quickly rotating the tube. After the required amount of blood was obtained, the tube was withdrawn and blood was collected into collection tube (BD microtainer tubes with K_2EDTA; BD biosciences; Franklin Lakes, NJ) and bleeding ceases by the eye pressure.

Hierarchical clustering, data visualization and Statistical Analysis

The staining scores resulted from IHC were converted into scaled values centered on zero (e.g., a score of 0 is converted to −2, 2 to 1, and 4 to 3) in Microsoft excel. The hierarchical analysis was performed using Cluster program (http://rana.lbl.gov/EisenSoftware.htm) with average linkage based on Pearson's correlation coefficient as the selection parameter on the unsupervised approach. The results were visualized using the Java TreeView software. The clustered data were arranged with markers on the horizontal axis and tissue samples on the vertical axis as recently described (8). Two biomarkers with a close relationship are located next to each other. Unpaired T-test was used to analyze the differences of tumor burden between experimental groups. Data analysis was performed with GraphPad Prism version 4.00 for Windows (GraphPad Software, San Diego, CA); p values < 0.05 were considered statistically significant.

Results and Discussion

To investigate whether inhibition of mTOR by rapamycin may represent a suitable targeted therapy for skin tumor lesions, we began by inducing the formation of tumors in mice by the topical application of a single dose of a carcinogen, DMBA, followed by the chronic application of tumor promoter, TPA. When mice (n=10) started developing skin tumoral lesions (9 weeks of TPA treatment, Fig. 1), they were divided into two groups, and treated with rapamycin or vehicle for 5 consecutive days. This treatment proved to be effective in diminishing the accumulation of the phosphorylated form of S6 (Fig. 1, lower panels), a direct downstream target of mTOR (17). The effect of rapamycin on the skin neoplasias was remarkable. While the number and size of the tumors continued to increase in the control animals, this five-days treatment with rapamycin was sufficient to decrease the tumor multiplicity and to induce complete tumor regression after 6 weeks (Fig. 1B).

All control mice had to be euthanized 25 weeks after starting the TPA treatment due to their weight loss (Fig 1A). In the rapamycin-treated group, some tumors began recurring 10 weeks after completing the rapamycin administration (week 19 of the chemical carcinogenesis protocol, Fig. 1B). To assess the efficacy of rapamycin on these recurring tumor lesions, we initiated a second phase of rapamycin treatment at week 24 (tumors n=15; 3.3±0.3mm), and extended the daily administration until the end of week 31 (tumors n=5; 3.1±0.7 mm). Even when these tumors had relapsed and were in a very advanced stage, rapamycin still reduced effectively their multiplicity (p=0.0001).

These results prompted us to investigate the anticancer effects of the rapamycin in advanced stages of tumor progression (control group 10 mice, tumors n=21, 3.1±0.3 mm; treatment group 10 mice, tumors n=22, 3.9±0.4 mm, Fig. 2). The response to rapamycin treatment was evident by the reduction of the tumor burden as early as one week after initiating the treatment, observing a gradual regression of the tumors thereafter. Vehicle-treated animals had to be sacrificed at week 6 after the initiation of vehicle administration due to the overwhelming tumor burden (tumors n=68, 3.8±0.4 mm). A total of 22 representative tumors were collected for further analysis, 12 of which were diagnosed histopathologically as papillomas, and 10 as SCC. At this particular time point the rapamycin-treated group showed a significant lower tumor burden (tumors n=13; 3.2±0.2 mm, p<0.0001) (Fig. 2). Representative tumors from each group at week 6 of treatment are shown in Fig. 2. Only few small tumors were still visible at the end of the study, which was terminated after 12 weeks of rapamycin treatment (tumors n=3, 2±0 mm). All tumors were diagnosed as papillomas. These results indicate that rapamycin also exerts a potent antitumoral effect in advanced stages of chemically induced SCC.

Because rapamycin and its derivatives (rapalogs) act as immunosuppressive drugs (18), we explored whether the antitumor effect of rapamycin was related to this pharmacological activity. IHC analysis of animals treated in parallel with vehicle control or rapamycin for a prolonged time (6 weeks), revealed that there was no significant decrease in the number of macrophages, as recently reported (19), and T-cells within the tumors and their surrounding tissues, suggesting that rapamycin does not affect the number of infiltrating inflammatory and immune cells in the tumor and stromal compartments (Table 1). Similarly, we did not see any significant reduction in the blood vessel density of these tumors, as judged by the use of anti-CD31 and -CD34 IHC to detect tumor endothelial cells (Supp. Fig. 1). On the other hand, analysis of blood samples from the animals exposed to rapamycin or vehicle for 6 weeks did not show any statistically significant difference in any of the blood cell components (Table 1). These data suggest that the antitumoral effects of rapamycin are not likely due to its anti-angiogenic effect or a reduction in the overall number of circulating and tumor-infiltrating immune cells.

The effectiveness of rapamycin in diminishing the tumor burden in this chemically-induced SCC model provided the opportunity to monitor and quantify the molecular signaling changes provoked by the treatment with rapamycin in a temporal manner. We focused on molecules related to the Akt/mTOR pathway (pS6, pAKT^{Ser473}, eIF4E), and biomarkers reflecting the status of cell metabolism, cell proliferation and cell death (p53, proliferating cell nuclear antigen (PCNA), cyclin D1 (CCND1), glucose transporter 1 (Glut1), and TUNEL assay), as well as tumor angiogenesis (VEGF). A decrease in the level of pS6 in rapamycin-treated tumors clearly contrasts the high level of pS6 in the control group (Fig. 3A), reflecting the hyperactivity of the AKT/mTOR signaling pathway in SCC (9, 20). Concomitant with a reduction in pS6, we noted a decrease in cell proliferation, as judged by staining for PCNA and a cell cycle regulating cyclin, CCND1 (Fig. 3A).

One of the key genetic aberrations of chemically induced SCC mouse model is the presence of mutations in the *p53* tumor suppressor gene (15), which was nicely reflected by the high level of p53 expression by IHC. The mutational status of the *p53* gene was confirmed by the sequence analysis of PCR-amplified genomic DNA from tumor samples from both control and rapamycin treated groups. Three out of 10 tumors from the control group exhibited heterozygous mutation of p53 (245R>L, 55E>K, and 68A>E), which is aligned with prior studies using a similar chemical carcinogenesis approach (21). Sequencing of *p53* from the rapamycin treated group revealed that 3 out of 7 tumors harbored heterozygous mutation of p53 (268E>Q, 239C>F, and 55E>K). Unexpectedly, however, we observed a reduction in the number of cells showing nuclear p53 in response to rapamycin treatment (Fig. 3A). This observation suggests that few days of rapamycin treatment may not be sufficient to eliminate the tumor cell population bearing *p53* mutations, but that these cells are sensitive to rapamycin, as previously reported (22), probably because mTOR inhibition may interfere with the expression of the mutant forms of p53 protein or may facilitate their degradation, an area that certainly warrant further investigation.

The non-supervised hierarchical class comparison of the IHC data (8) revealed a strong temporal relationship among most of the samples in response to rapamycin treatment. For example, as shown in Fig. 3B, all control samples clustered together, and tissues collected after one day of treatment were adjacent to them. All samples collected after 3 days clustered together. All samples from animals treated for 5 and 7 days were closely clustered. From the heat-map approach, it was clear that rapamycin began to be effective after one day of treatment and even more effective after 3 days, as judged by the decreased in pS6. This was partially reflected by a gradual decreased in the phosphoylation on Akt in serine 473, a target for the mTOR complex 2 (mTORC2) (20). Indeed, pS6 and pAkt^{Ser473} clustered together in this analysis. This was only partially related to a smaller and slower decrease in

the levels of VEGF, which may explain the limited impact of rapamycin in tumor angiogenesis in these aggressive chemically-induced tumors, in contrast to results obtained in xenograft models (9).

Of interest was also the observation that proliferative makers (cyclin D1 and PCNA) clustered together, in close relationship to p53, all of which began to be reduced with respect to controls after 5-7 days of treatment. The immunodetection of Glut1, which reflects an increased glucose metabolism (23), was more closely related to these molecules than to pS6, suggesting an interesting relationship between the metabolic state of the cells and their proliferative capacity. In contrast, the levels of eIF4E were not affected by the rapamycin treatment, and served as an internal control. Similarly, whereas we have observed a rapid decrease in the levels of phosphorylated 4E-BP1, a downstream target of mTOR that represses eIF4E-dependent translation (24), in HNSCC cells exposed to rapamycin (9), we did not observe a reproducible decrease of phosphorylated 4E-BP1 in chemically-induced epithelial SCC upon rapamycin treatment (not shown). This observation raises the possibility that kinases other than mTOR may phosphorylate 4E-BP1 in SCC cells, including members of the MAP kinase (MAPKs) and cyclin-dependent kinase (CDK) superfamily, as previously reported (25-27), which may account for the rapamycin insensitivity of the phosphorylation of 4E-BP1. On the other hand, we also noticed that this clustering analysis divided the data into two separated groups at day 3 after rapamycin treatment (Fig. 3B). This is likely because in parallel with the anti-proliferative effects of rapamycin, we also observed areas of massive apoptotic cell death on day 3 in the rapamycin-treated group, as revealed by TUNEL labeling assays (Fig. 3C). Thus, rapamycin appears to cause the rapid inhibition of mTOR and a consequent reduction in pS6 and $pAKT^{Ser473}$. This is then followed by the apoptotic death of a fraction of the cancer cells and the reduction in the cell proliferation of the surviving ones, with a concomitant decrease in the population of cancer cells expressing high levels of mutant p53.

The increased molecular understanding of cancer has provided a wealth of opportunity for identifying novel therapies targeting molecular mechanisms that are dysregulated in particular cancer types. For example, in the case of SCC from the head and neck, recently available evidence indicates that activation of the Akt-mTOR signaling pathway is a widespread event, likely independently of the level of activation of EGFR and the mutational status of p53 (8, 9). The use mTOR inhibitors for the treatment of SCC could therefore represent a suitable approach. However, it is imperative to validate further the effectiveness of candidate drugs using animal models that reflect the complexity of the human disease better than classical xenograft models, before pursuing their clinical evaluation in SCC patients. Indeed, while many differences between human cancers and chemically induced tumors in mice exist (12, 15), the classical two-stage chemical carcinogenesis model involving a tobacco carcinogen (DMBA) and the pro-proliferative effect of a tumor promoter (TPA) creates an environment permissive for cancer development leading to progressive squamous epithelial tumors that resemble human squamous cancers (28). In particular, using this model we observed that rapamycin is effective in halting the tumor progression, and causes the regression of both early papillomas and more advanced SCC, including those exhibiting mutant p53, thus reducing dramatically the tumor burden of tumor-bearing mice.

Together with the promising antitumoral activity of rapamycin and its analogs, CCI-779 and RAD001, in breast cancer, glioblastoma and mantle cell lymphoma patients (18, 20), and the recent approval by the FDA of the use of CCI-779 (temsirolimus) in advanced renal carcinoma (29), our present findings provide a strong rationale for the early evaluation of mTOR inhibitors as a molecular targeted approach to treat SCC. Furthermore, the ability to investigate the relationship among molecular changes caused by mTOR inhibition by

conventional IHC, may now provide a number of biological relevant biomarkers that can be used to monitor the effectiveness of mTOR inhibition in cancerous tissues in response to rapamycin and its analogs in the clinical setting.

Supplementary Material

Refer to Web version on PubMed Central for supplementary material.

Bibliography

1. Vogelstein B, Kinzler KW. Cancer genes and the pathways they control. Nat Med. 2004; 10:789–99. [PubMed: 15286780]
2. Forastiere A, Koch W, Trotti A, Sidransky D. Head and neck cancer. N Engl J Med. 2001; 345:1890–900. [PubMed: 11756581]
3. Patel V, Rosenfeldt HM, Lyons R, et al. Persistent activation of Rac1 in squamous carcinomas of the head and neck: evidence for an EGFR/Vav2 signaling axis involved in cell invasion. Carcinogenesis. 2007; 28:1145–52. [PubMed: 17234718]
4. Pomerantz RG, Grandis JR. The role of epidermal growth factor receptor in head and neck squamous cell carcinoma. Curr Oncol Rep. 2003; 5:140–6. [PubMed: 12583831]
5. Dorsam RT, Gutkind JS. G-protein-coupled receptors and cancer. Nat Rev Cancer. 2007; 7:79–94. [PubMed: 17251915]
6. Shaw RJ, Cantley LC. Ras, PI(3)K and mTOR signalling controls tumour cell growth. Nature. 2006; 441:424–30. [PubMed: 16724053]
7. Amornphimoltham P, Sriuranpong V, Patel V, et al. Persistent activation of the Akt pathway in head and neck squamous cell carcinoma: a potential target for UCN-01. Clin Cancer Res. 2004; 10:4029–37. [PubMed: 15217935]
8. Molinolo AA, Hewitt SM, Amornphimoltham P, et al. Dissecting the Akt/mammalian target of rapamycin signaling network: emerging results from the head and neck cancer tissue array initiative. Clin Cancer Res. 2007; 13:4964–73. [PubMed: 17785546]
9. Amornphimoltham P, Patel V, Sodhi A, et al. Mammalian target of rapamycin, a molecular target in squamous cell carcinomas of the head and neck. Cancer Res. 2005; 65:9953–61. [PubMed: 16267020]
10. Nathan CO, Amirghahari N, Rong X, et al. Mammalian target of rapamycin inhibitors as possible adjuvant therapy for microscopic residual disease in head and neck squamous cell cancer. Cancer Res. 2007; 67:2160–8. [PubMed: 17332346]
11. Wislez M, Spencer ML, Izzo JG, et al. Inhibition of mammalian target of rapamycin reverses alveolar epithelial neoplasia induced by oncogenic K-ras. Cancer Res. 2005; 65:3226–35. [PubMed: 15833854]
12. Frese KK, Tuveson DA. Maximizing mouse cancer models. Nat Rev Cancer. 2007; 7:645–58. [PubMed: 17687385]
13. Lu SL, Herrington H, Wang XJ. Mouse models for human head and neck squamous cell carcinomas. Head Neck. 2006; 28:945–54. [PubMed: 16721744]
14. Becher OJ, Holland EC. Genetically engineered models have advantages over xenografts for preclinical studies. Cancer Res. 2006; 66:3355–8. discussion 8-9. [PubMed: 16585152]
15. DiGiovanni J. Multistage carcinogenesis in mouse skin. Pharmacol Ther. 1992; 54:63–128. [PubMed: 1528955]
16. Charafe-Jauffret E, Tarpin C, Bardou VJ, et al. Immunophenotypic analysis of inflammatory breast cancers: identification of an ‘inflammatory signature’. J Pathol. 2004; 202:265–73. [PubMed: 14991891]
17. Affara NI, Trempus CS, Schanbacher BL, et al. Activation of Akt and mTOR in CD34+/K15+ keratinocyte stem cells and skin tumors during multi-stage mouse skin carcinogenesis. Anticancer Res. 2006; 26:2805–20. [PubMed: 16886599]
18. Vignot S, Faivre S, Aguirre D, Raymond E. mTOR-targeted therapy of cancer with rapamycin derivatives. Ann Oncol. 2005; 16:525–37. [PubMed: 15728109]

19. Granville CA, Warfel N, Tsurutani J, et al. Identification of a highly effective rapamycin schedule that markedly reduces the size, multiplicity, and phenotypic progression of tobacco carcinogen-induced murine lung tumors. Clin Cancer Res. 2007; 13:2281–9. [PubMed: 17404113]
20. Guertin DA, Sabatini DM. Defining the Role of mTOR in Cancer. Cancer Cell. 2007; 12:9–22. [PubMed: 17613433]
21. Ruggeri B, Caamano J, Goodrow T, et al. Alterations of the p53 tumor suppressor gene during mouse skin tumor progression. Cancer Res. 1991; 51:6615–21. [PubMed: 1742735]
22. Huang S, Liu LN, Hosoi H, Dilling MB, Shikata T, Houghton PJ. p53/p21(CIP1) cooperate in enforcing rapamycin-induced G(1) arrest and determine the cellular response to rapamycin. Cancer Res. 2001; 61:3373–81. [PubMed: 11309295]
23. Gatenby RA, Gillies RJ. Why do cancers have high aerobic glycolysis? Nature Reviews Cancer. 2004; 4:891–9.
24. Mamane Y, Petroulakis E, LeBacquer O, Sonenberg N. mTOR, translation initiation and cancer. Oncogene. 2006; 25:6416–22. [PubMed: 17041626]
25. Mothe-Satney I, Brunn GJ, McMahon LP, Capaldo CT, Abraham RT, Lawrence JC Jr. Mammalian target of rapamycin-dependent phosphorylation of PHAS-I in four (S/T)P sites detected by phospho-specific antibodies. J Biol Chem. 2000; 275:33836–43. [PubMed: 10942774]
26. Wang X, Li W, Parra JL, Beugnet A, Proud CG. The C terminus of initiation factor 4E-binding protein 1 contains multiple regulatory features that influence its function and phosphorylation. Mol Cell Biol. 2003; 23:1546–57. [PubMed: 12588975]
27. Heesom KJ, Gampel A, Mellor H, Denton RM. Cell cycle-dependent phosphorylation of the translational repressor eIF-4E binding protein-1 (4E-BP1). Curr Biol. 2001; 11:1374–9. [PubMed: 11553333]
28. Balmain A, Pragnell IB. Mouse skin carcinomas induced in vivo by chemical carcinogens have a transforming Harvey-ras oncogene. Nature. 1983; 303:72–4. [PubMed: 6843661]
29. Hudes G, Carducci M, Tomczak P, et al. Temsirolimus, interferon alfa, or both for advanced renal-cell carcinoma. N Engl J Med. 2007; 356:2271–81. [PubMed: 17538086]

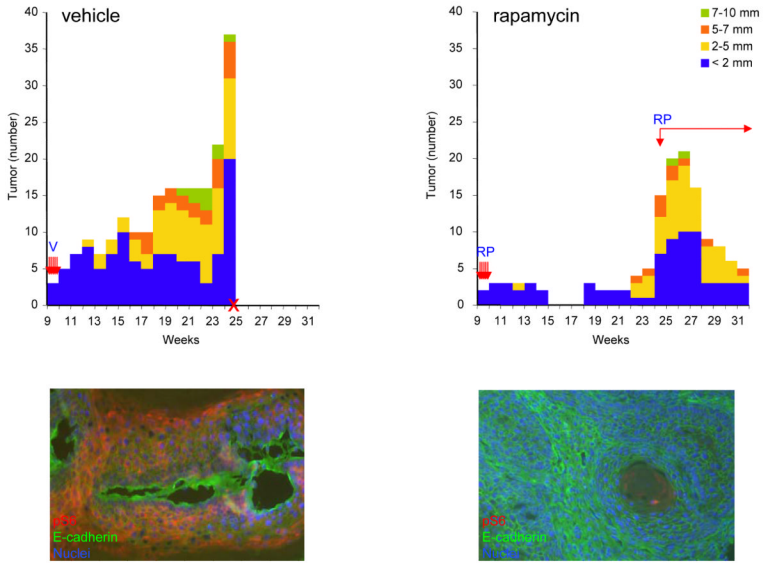

Figure 1.

Anti-tumoral effects of rapamycin in early lesions of chemically-induced skin tumors. Mice were treated with a single dose of the carcinogen DMBA (initiation), followed by the twice weekly treatment with TPA (promotion). The number and diameter of each tumor was measured weekly, and plotted as a function of time (weeks) after the exposure to DMBA. Rapamycin (RP; 10 mg/kg) or vehicle (V) treatment started at week 9. The second phase of the rapamycin treatment in the rapamycin-treated group was reinitiated at week 24, as indicated. *Bar*, number of tumors of each size (indicated by color coding). *Arrows*, rapamycin treatment. X, week in which mice had to be sacrificed due to their tumor burden. Representative IF analysis of the tissues from the corresponding vehicle and rapamycin treated animals. The phosphoS6 (*pS6*; in red) immunodetection reflected the mTOR status and *E-cadherin* (in green) was used to label tumor cells. Cell nuclei were stained with DAPI (in blue).

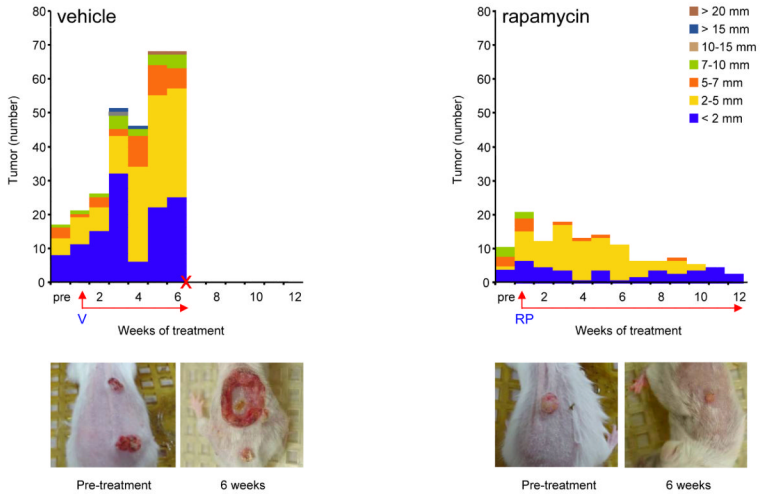

Figure 2.

Antitumoral effect of rapamycin in advanced skin cancer lesions.

The number and size of chemically-induced tumors in mice treated with vehicle (V) and rapamycin (RP; 10 mg/kg) was depicted as for Figure 1. *Bar*, number of tumors of the indicated size based on their designated color coding. Rapamycin treatment was initiated when most of the animals had at least 1-2 large tumors, as indicated. The control group had to be sacrificed 6 weeks after treatment initiation with vehicle, as indicated with an X. *Arrows*, (RP) rapamycin or (V) vehicle treatment. Representative tumors were photographed before rapamycin initiation (Pre-treatment) and after 6 weeks of the initial treatment with rapamycin or vehicle control.

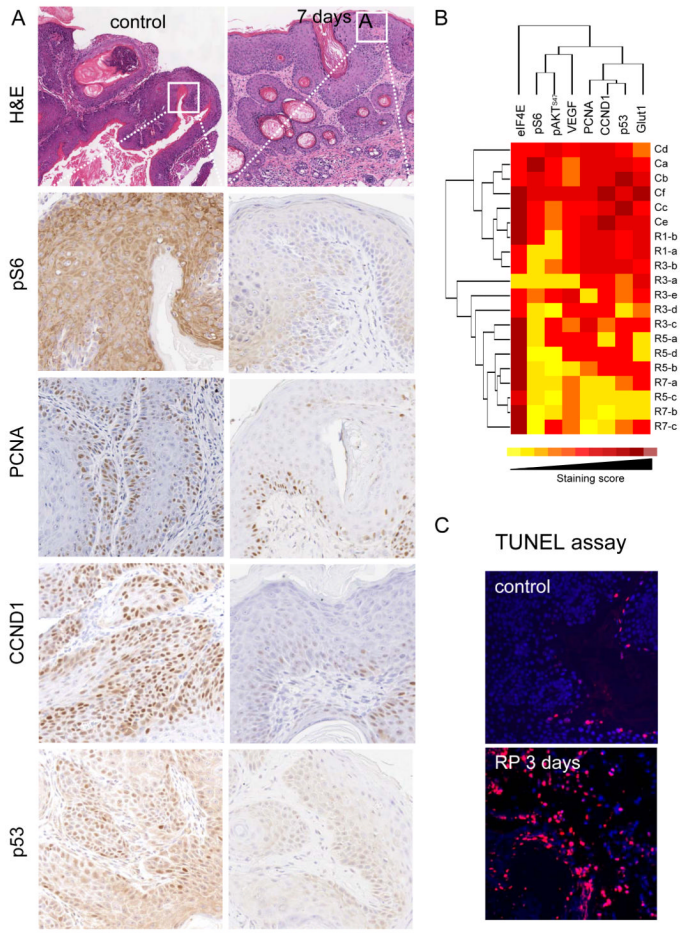

Figure 3.

Immunohistochemical analysis of biomarkers of rapamycin treatment response. *A*. IHC from representative tumors acquired from control and rapamycin-treated mice 7 days after initiating the rapamycin treatment as described in Figure 2. The antibodies used are indicated. *B*. Hierarchical clustering of IHC staining score against different biomarkers from the control tumors (C) and the papillomas harvested at different time points after rapamycin administration (R1, day 1; R3, day 3; R5, day 5; and R7, day 7). *Deep red*, high staining scores (strong staining intensity and 75-100% of positive staining cells). *Yellow*, low staining scores (weak staining intensity and less than 10% of cells positive for IHC). *C*. TUNEL staining showing the apoptotic cells (in red) of tumor sections from the control and rapamycin-treated mice after 3 days of the rapamycin treatment initiation. Cell nuclei were stained with DAPI (in blue).

Table 1

Complete blood count and immunohistochemistry (IHC) results from vehicle and rapamycin-treated animals Blood samples were collected from mice at advanced stages of tumor progression, as described in Figure 2, after prolonged (6 weeks) treatment with rapamycin and vehicle (see Materials and Methods). Standard complete blood cell components were analyzed. WBC (white blood cells), RBC (red blood cells), MCV (mean corpuscular volume), Polys (polymorphonuclear leukocytes). IHC for T cells markers (CD3+) and macrophage markers (F4/80+) were analyzed in tissue from the corresponding vehicle and rapamycin treated animals. Numbers are the mean (average) ± standard error of the mean.

Blood	**Vehicle Average (n=7)**	**Rapamycin Average (n=7)**
WBC count (K/μL)	10.4 (4.7)	11.4 (4.7)
RBC count (M/μL)	6.3 (2.8)	7.2 (2.9)
Hemoglobin (g/dL)	11.3 (5.1)	12.7 (5.2)
Hematocrit (%)	33.7 (15.1)	35.1 (14.3)
MCV (fL)	57.4 (25.7)	49.9 (20.4)
Platelets (K/μL)	1437.6 (642.9)	1125.0 (459.3)
Polys (%)	44.7 (20.0)	37.1 (15.1)
Lymphocytes (%)	44.3 (19.8)	43.6 (17.8)
Monocytes (%)	8.7 (3.9)	15.9 (6.5)
Eosinophils (%)	0.9 (0.4)	0.5 (0.2)
Basophils (%)	1.6 (0.7)	3.0 (1.2)
Tumor tissues (IHC)	**Vehicle Average* (n=5)**	**Rapamycin Average* (n=5)**
T cells (CD3+)	96.4 (17.1)	97.6 (11.8)
Macrophage (F4/80+)	221.6 (10.5)	230.8 (41.2)

* arbitrary unit